H-mode access and performance in the Mega-Amp Spherical Tokamak

R. J. Akers, J. W. Ahn, L. C. Appel, E. R. Arends, K. B. Axon et al.

Citation: Phys. Plasmas **9**, 3919 (2002); doi: 10.1063/1.1490928
View online: http://dx.doi.org/10.1063/1.1490928
View Table of Contents: http://pop.aip.org/resource/1/PHPAEN/v9/i9
Published by the American Institute of Physics.

H-mode access and performance in the Mega-Amp Spherical Tokamak[a)]

R. J. Akers,[b)] J. W. Ahn,[c)] L. C. Appel, E. R. Arends,[d)] K. B. Axon, R. J. Buttery, C. Byrom,[e)] P. G. Carolan, G. F. Counsell, G. Cunningham, D. Ciric, N. J. Conway, J. Dowling, A. R. Field, S. J. Fielding, S. Gee, M. P. Gryaznevich, M. Hole, A. Kirk, I. Lehane,[f)] B. Lloyd, S. Manhood, R. Martin, G. McArdle, M. McGrath,[g)] H. Meyer, A. W. Morris, M. P. S. Nightingale, T. Pinfold, M. Price, C. Ribeiro, V. Shevchenko, S. Shibaev, A. Sykes, A. Tabasso, D. Taylor, M. R. Tournianski, M. Valovič, M. J. Walsh,[h)] S. E. V. Warder, J. R. Watkins, H. R. Wilson, S. You,[c)] and the MAST and NBI teams

EURATOM/UKAEA Fusion Association, Culham Science Center, Abingdon, Oxon, OX14 3DB, United Kingdom

(Received 15 March 2002; accepted 29 April 2002)

Spontaneous transitions from the low ''L-mode'' to high ''H-mode'' of tokamak plasma confinement, first observed during neutral beam heating experiments on ASDEX, are now routinely achieved in many tokamak experiments. The H-mode regime is attractive as it offers the possibility of enhanced confinement, and thus a route towards a more ''compact'' and cost-efficient fusion power-plant. Transition to H-mode is now routinely achievable in the Mega-Amp Spherical Tokamak (MAST) [A. C. Darke *et al.*, *Fusion Technology 1994* (Elsevier, Amsterdam, 1995), Vol. 1, p. 799] for both Ohmically and neutral beam injection (NBI) heated plasmas ($P_{\mathrm{NBI}}\sim 0.5$–1.7 MW). H-mode plasmas can be either center stack limited or X-point diverted, exhibiting regular Type III edge localized modes (ELMs). Global confinement in H-mode with low frequency ELMs is consistent with the international IPB(y,2) scaling and exceeds the scaling by a factor ~ 1.5–2.0 for high performance discharges. Confinement degrades with increasing ELM frequency (which in turn scales with power and density) as for conventional tokamaks. Densities above the Greenwald limit ($G\sim 1$) have been achieved for plasma currents up to 0.8 MA using gas-fueling, and up to 0.9 MA using a low field side multi-pellet injector. High field side fueling, on the other hand, can be supplied via a gas-feed located at the center-column mid-plane, this technique having been found to dramatically enhance H-mode accessibility and quality. When combined with Connected Double Null plasma topology, a significant reduction in Ohmic L–H power threshold can be achieved; as a result, power threshold data are now in broad agreement with a number of the latest scaling law predictions. Following the transition to H-mode, power crossing the inner separatrix remains low, resulting in a high recycling scrape-off layer (compared with partial detachment in L-mode). To date, with NBI power limited to 1.7 MW, H-mode MAST plasmas have shown no evidence of having approached a beta limit ($\beta_N\sim 4.5 l_i$). High performance H-mode discharges are at sufficient poloidal beta (β_p), however, to enable the first studies of the Neoclassical Tearing Mode, the MHD instability responsible for limiting the achievable beta in conventional tokamaks. [DOI: 10.1063/1.1490928]

I. INTRODUCTION

MAST (the Mega-Amp Spherical Tokamak) (Ref. 1) (shown schematically in Fig. 1 together with the operational parameters achieved to date listed in Table I) is a large, second generation Spherical Tokamak (ST) (Ref. 2) capable of producing low collisionality, low aspect ratio ($A=R/a\sim 1.4$), highly elongated plasmas (elongation $\kappa>2$) with a poloidal cross section comparable to DIII-D and ASDEX-U. The operating space spanned by MAST was extended in 2001, and 1 MA plasmas with a flat-top duration of 200 ms can now be routinely generated. Greenwald numbers$=\bar{n}_{e20}\pi a^2/I_p$) exceed 1.0 for discharges with plasma currents (I_p) up to 0.8 MA using gas fueling, and up to 0.9 MA using deuterium pellet injection. H-mode (or high confinement mode) access is routine for both Ohmic and Neutral Beam Injection (NBI) heated discharges, aided mainly by the installation of an inboard gas-feed [~35% of discharges in the 2001 campaign contained regular edge localized modes (ELMs)]. It is therefore now possible to study the ST H-mode in detail. In Sec. II we discuss H-mode access and performance, in

[a)]This paper is based on an invited talk at the 2001 APS DPP Meeting, Long Beach, CA, Paper LI1 1, Bull. Amer. Phys. Soc. **46**, 206 (2002).

[b)]Invited speaker. Electronic mail: rob.akers@ukaea.org.uk

[c)]Also at the Imperial College of Science, Technology and Medicine, University of London, London, SW7 2BZ, United Kingdom.

[d)]Also at the FOM Instituut voor Plasmafysica ''Rijnhuizen,'' Postbus 1207, 3430 BE Nieuwegein, The Netherlands.

[e)]Also at the Physics Department, UMIST, P.O. Box 88, Manchester M60 1QD, United Kingdom.

[f)]Also at the Department of Physics, National University of Ireland, University College Cork, Ireland.

[g)]Also at the Department of Experimental Physics, University College Dublin, Belfield, Dublin 4, Ireland.

[h)]Also at the Walsh Scientific Ltd., Abingdon, Oxon, OX14 3EB, United Kingdom.

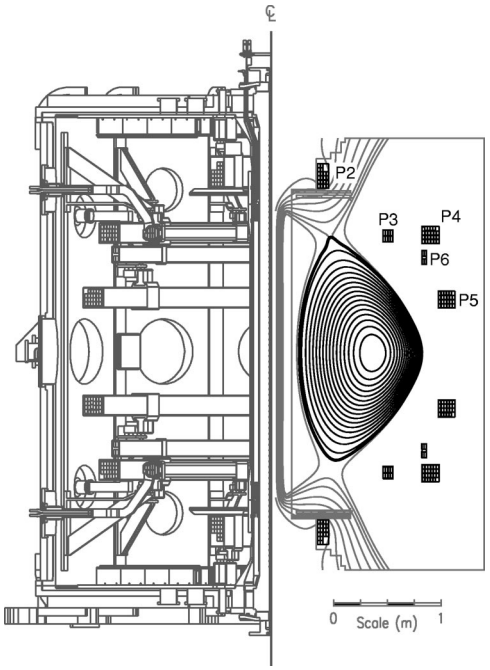

FIG. 1. Engineering drawing of MAST (left) with an upper single null diverted EFIT equilibrium (right).

particular core confinement and ELM phenomenology for Ohmic and NBI heated H-mode discharges. Section III describes power handling, detailing new results concerning detachment, in–out separatrix power asymmetries and the latest results from a newly installed mid-plane reciprocating probe. In Sec. IV we discuss current operational limits; in particular, we concentrate on the fueling of H-mode plasmas and attempts at increasing the achievable density using a mid-plane mounted multi-pellet injector. Finally, in Sec. V we briefly address the stability of plasmas generated to date, concentrating on the first observations of the Neoclassical Tearing Mode (NTM) (Refs. 3 and 4) in the Spherical Tokamak, made possible due to the high poloidal betas (β_p) achieved in low collisionality H-mode plasmas. A summary is provided in Sec. VI.

II. H-MODE ACCESS AND PERFORMANCE

Early attempts at accessing H-mode in MAST required loading of the plasma facing surfaces with deuterium by first generating a density limited discharge. The resulting plasmas demonstrated all of the established H-mode signatures, i.e., an increase in particle and energy confinement, steepening of the edge gradients and a sharpening of the D_α profile at the plasma periphery. In addition, a reduction in turbulence was observed, together with a dramatic increase in the Electron Bernstein Wave (EBW) emission cone and the onset and saturation of edge poloidal flow, results being reported in Ref. 5. There were, however, competing constraints concerning the inner gap between the plasma and center column armor: too small a gap and excessive carbon influx is thought to have occurred, too large a gap and the fueling efficiency is believed to have been compromised. In order to provide greater flexibility, control and reproducibility, an inboard gas-feed, similar to the system developed for COMPASS-D (Ref. 6) has been installed. The feed tube itself has a 3 mm bore and runs under the center column armor from the top of the vessel to an outlet in the mid-plane of the machine. D_2 gas is supplied at $\leqslant 10$ bar via a pneumatic valve, constant flow being achieved after $\sim$50 ms at typically $\sim$60 mbl/s (3×10^{21} atoms/s) for 2 bar inlet pressure. This alone is sufficient to sustain the plasma density (typically $nV/\tau_P \sim 3.5\times10^{21}$ atoms/s where V is the plasma volume and τ_P the particle confinement time). As a result, NBI heated H-mode plasmas can now be generated in center column limited, and reliably for Double Null Diverted (DND) discharges without prior wall loading. In addition, Ohmically heated H-mode plasmas can now be accessed in carefully balanced, Connected Double Null (CDN) diverted plasmas. Here, we define the CDN topology for $\Delta_{sep}/\rho_i < 0.5$ where Δ_{sep} is the distance at the outboard mid-plane between flux surfaces corresponding to the upper and lower X-points and ρ_i is the thermal ion Larmor radius. A more detailed synopsis of the MAST inboard gas-feed and resulting physics can be found in Ref. 7.

Pseudo steady-state ELMing H-mode discharges are typically sustained for a duration of $\sim$200 ms at I_p up to 1 MA, even at densities approaching the Greenwald limit. Typical plasma parameters are toroidal field $B_\phi \sim 0.53$ T, $I_p \sim 0.8$ MA, loop voltage (at the inboard mid-plane) $V_l \sim 1.5$ V, safety factor $q_{95} \sim 5$, major radius R$\sim$0.8 m and minor radius $a \sim 0.6$ m. Line average Z_{eff} during the 2001 campaign, determined via visible bremmstrahlung emission, was typically $\sim$1.5 at moderate to high density ($>5\times10^{19}$ m^{-2}), rising to between 2.0 and 4.0 at low density $\sim 2\times10^{19}$ m^{-2}). Figure 2 shows the existence space in terms of plasma current and line average electron density ($\bar{n}_e$) for shot numbers #4100–4600. Here, low confinement (L-mode) discharges (black) have been overlaid by H-mode plasmas (gray). The H-mode window is broader than the equivalent operating space on the Small Tight Aspect Ratio Tokamak (START) (reported in Ref. 8, also shown here) where good beam absorption could only be achieved in a narrow density window and at the highest possible plasma currents ($\sim$0.3 MA). H-mode plasmas on MAST clearly represent the highest performance discharges so far achieved on MAST.

Figure 3 shows traces for shot #4161, a typical NBI heated H-mode discharge. The inboard gas puff provided a D_2 flux of 10^{21}/s from the start (the outboard gas puff was

TABLE I. MAST and START parameters.

	MAST		START
	Design	Achieved	
Minor and major radii a,R (m)	0.65,0.85	0.65,0.85	0.25,0.32
κ (elongation)	$\leqslant$3	2.2	$\leqslant$3
Aspect ratio (R/a)	$\geqslant$1.3	1.3	$\geqslant$1.2
Plasma and TF rod current	2, 2.2	1.1,2.2	0.31, 0.5
Toroidal field at R (T)	0.52	0.51	0.31
Auxiliary heating: P (NBI) (MW)	5	2	1
P (ERCRH) [MW]	1.4	0.6	0.2
Pulse length (s)	1-5	0.5	$\leqslant$0.06
Plasma volume (m^3)	10	10	0.5

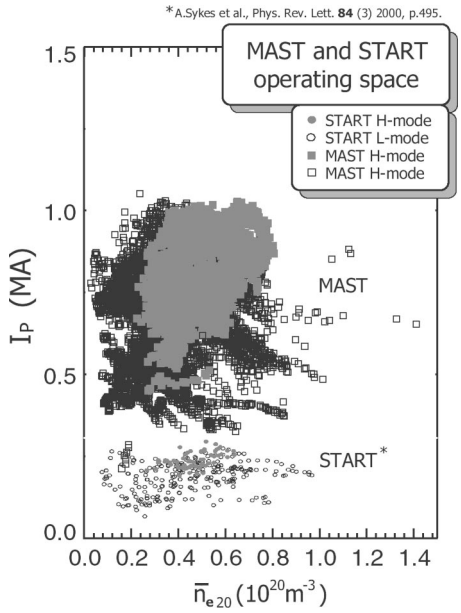

FIG. 2. MAST and START operating space for L-mode and H-mode plasmas in terms of achievable plasma current and line average electron density.

only used in the plasma formation phase). A plasma current of 0.9 MA was sustained for 200 ms with an applied loop voltage at the inner separatrix of 1.3 V, together with 1.1 MW of hydrogen beam injection. The precipitous decrease in soft X-ray (SXR) emission at 60 ms is thought to have resulted from the appearance of the $q=2$ rational surface and was accompanied by a 2/1 snake. 50 ms later, the programmed decrease in applied loop voltage appears to have triggered a L–H transition followed by the onset and sustainment for ~180 ms of ''regular'' ELMs (in contrast to the lower density discharges reported in Ref. 5 which contained sporadic, possibly Type-I, ELMs). A significant increase in stored energy up to 70 kJ was observed and despite the pres-

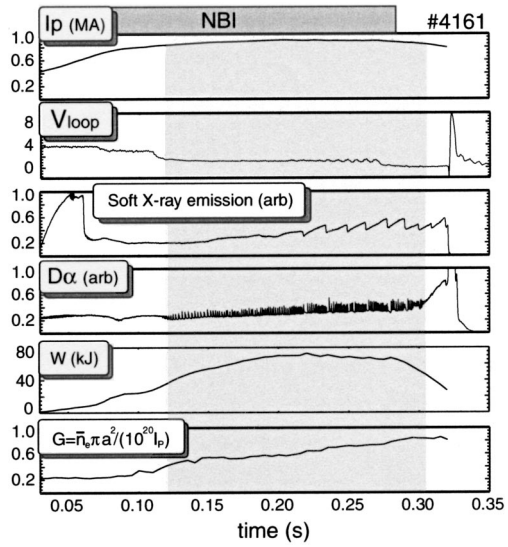

FIG. 3. Temporal evolution of various plasma parameters for H-mode discharge #4161. The H-mode phase of the discharge is shaded.

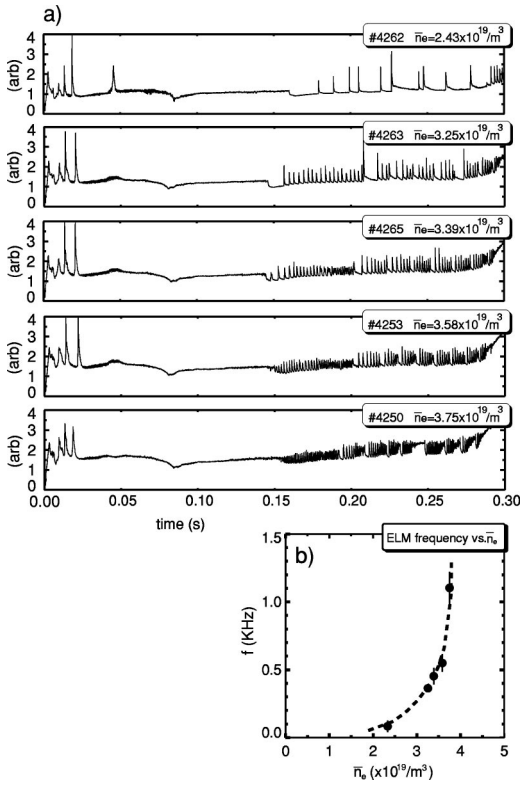

FIG. 4. (a) D_α emission for a series of typical H-mode discharges. Here, only the density was chosen to vary. ELM frequency at H-mode onset is positively correlated with line average density as shown in (b).

ence of the rapid ELMs, the density continued to rise to $G \sim 1$ over a period of 190 ms.

The achievement of routine H-mode access for plasmas with ''regular'' ELMs, for the first time in a ST provides a valuable comparison with the conventional tokamak ELMy H-mode. For instance, it is now possible to study the correlation between ELM frequency and various bulk plasma parameters. D_α traces for an ELMy H-mode density scan series (#4250–#4262), with nominal parameters $I_p \sim 750$ kA, $B_\phi \sim 0.45$ T, $A \sim 1.5$ and ~1 MW of auxiliary H-NBI heating are shown in Fig. 4. The temporal evolution of the D_α emission in the L-mode phase is highly repeatable (note, for example, the series of instabilities in the ramp phase, $t < 0.02$ s). Following the L–H transition, plasmas cease to be similar and a correlation between ELM frequency and onset line average density is observed [demonstrated more clearly in Fig. 4(b) where ELM frequency is plotted against $\bar{n}_e$)]. A similar experiment has been performed, where the input auxiliary heating (rather than the density) was scanned. In this case, a dramatic drop in ELM frequency was observed as the power crossing the separatrix was gradually increased, a feature characteristic of Type III ELMs at a conventional aspect ratio (see, for example, Ref. 9).

A significant advance in the latest campaign of experiments is that H-mode plasmas can now be accessed using Ohmic heating alone, thus allowing access criteria to be studied at the lowest achievable input power. To eliminate the question of whether the plasma is, or is not in H-mode in the presence of very high frequency ELMs close to transition

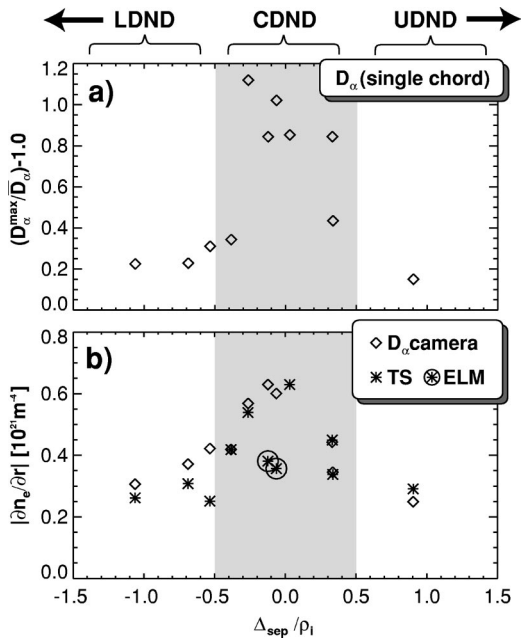

FIG. 5. (a) H-mode "depth" parameter Q_{H} versus normalized separatrix distance $\Delta_{\mathrm{sep}}/\rho_i$ (CDND regime shown shaded). (b) Edge density gradient versus $\Delta_{\mathrm{sep}}/\rho_i$ measured using the mid-plane D_α array ($\diamond$) and the 300 spatial point Thomson Scattering system (*). Circled points are for data taken on-ELM.

(threshold or Type III ELMs), various parameters can be defined which quantify the "depth" or "quality" of the H-mode. One such parameter is the confinement time, another is the confinement H-factor H_{H}; close to threshold, however, the increase in H_{H} or τ_E is only marginal. Instead, we choose a parameter Q_{H}, defined by the maximum to mean D_α signal $Q_{\mathrm{H}}=(D_\alpha^{\max}/\overline{D_\alpha})-1$. Larger ELMs, larger ELM free periods or lower inter-ELM D_α emission are thus expressed as an increase in Q_{H}.

Figure 5(a) shows Q_{H} plotted versus normalized separatrix distance $\Delta_{\mathrm{sep}}/\rho$ for 11 discharges. Data clearly demonstrate that higher quality "deep" Ohmic H-mode is more readily accessed (at constant power) in carefully balanced CDN diverted plasmas (i.e., when Δ_{sep} is within $\sim$1/2 an ion Larmor radius). The choice of ρ_i as a normalizing quantity is designed to allow cross-machine comparisons (ρ_i here remained approximately constant at $\sim$6 mm).

A second indicator of H-mode depth, the edge electron density gradient, is plotted [Fig. 5(b)] for the same series of discharges. Two independent methods for determining the edge gradient have been deployed; diamond polymarkers ($\diamond$) represent calculations based upon the radial width of the D_α emission layer (using a mid-plane D_α array) and asterisk shaped polymarkers (*) are based upon fits to the 300 spatial point Thomson scattering profile. Circled points are for discharges where the 30 ns laser pulse fired during an ELM, indicating a sudden collapse of the edge gradient down to L-mode levels. Both diagnostics show a marked increase in the H-mode edge density gradient when the plasma becomes CDN diverted (with a gradient $\sim$2 times the L-mode level for $\Delta_{\mathrm{sep}}\sim 0.0$).

A more detailed description of this work can be found in Ref. 10 and a similar observation by DIII-D in Ref. 11 (although not with resolution at the Larmor radius level), where high triangularity ($\delta\sim 0.8$), DIII-D plasmas are shown to exhibit the lowest power threshold for DND rather than SND plasmas (MAST plasmas having $\delta\sim 0.4$).

By combining in-board gas puffing with an adherence to the CDN diverted topology, a significant reduction in the L–H power threshold compared with that reported in Ref. 5 has been achieved (and hence access to the H-mode using Ohmic heating alone). Power threshold data for a subset of MAST *Ohmic* H-mode plasmas (where the density was the only parameter allowed to vary) are shown in Fig. 6. The figure shows a plot of the ratio of power crossing the separatrix at the L–H transition, P_{LH} to various scaling law predictions (see Refs. 12, 13, and 14), plotted against measured power. Here, P_{LH} has been determined using EFIT; the same conclusions can be drawn using Langmuir Probe and bolometry data (for Ohmic discharges, the agreement between the two is to better than 20% assuming scrape-off layer electron–ion equipartition). For these plasmas, the radiated power is typically 10–15% of total power crossing the separatrix P_{sep} and has not been subtracted. The coefficients and power indices of the various scaling laws are tabulated in the figure in the same format as Table 2, p. 2196, Chap. 2 of the ITER Physics basis (Ref. 13). For example, scaling 1 corresponds to $P_{\mathrm{LH}}=0.650 n_e 20^{0.93} B_T^{0.86} R^{2.15}$, with units [MW], [$10^{20}$ m^{-3}], [T] and [m]. Of particular note is that the latest international scalings (Ref. 14, shown in red), are in reasonable agreement with the latest MAST data, some $\sim$6 times closer than the EPS97 scaling prediction (Ref. 12) (although there remains a systematically increasing discrepancy as the plasma density increases). Data thus indicate that on MAST, the L–H power threshold is better represented by $P_{\mathrm{th}}\propto aR$ (i.e., the separatrix surface area at fixed κ) rather than $P_{\mathrm{th}}\propto R^2$. It is important to stress, however, that the MAST data are for low aspect ratio, DND Ohmic discharges with an open divertor structure (i.e., quite different to the majority of plasmas used to develop the scalings). In addition, it may well be that the minimum power required to achieve H-mode access is even lower, since the trigger here is clearly the change in magnetic configuration. Nevertheless, power threshold data from MAST will for the first time allow the aspect ratio to be included in the ITPA cross machine power threshold regression analysis, data shown here having recently been merged into the database.

Access to a regularly ELMing H-mode is a significant step forward for the ST, and is enabling a better comparison of MAST H-mode energy confinement with international scalings developed at a conventional aspect ratio. From the data discussed so far, it is clear that MAST discharges exhibit a wide range in ELM frequency, resulting from the broad range of densities and heating power. It is interesting therefore to plot confinement factor H_{H} (with respect to the international IPB98(y,2) scaling) against ELM frequency [Fig. 7(a)], in order to assess to what extent ELMs degrade confinement. For completeness, the 2001 confinement diagram [measured thermal confinement time versus scaling IPB98(y,2)] is also shown [Fig. 7(b)] for the latest high performance NBI heated plasmas. Blue points in Fig. 7(a) are

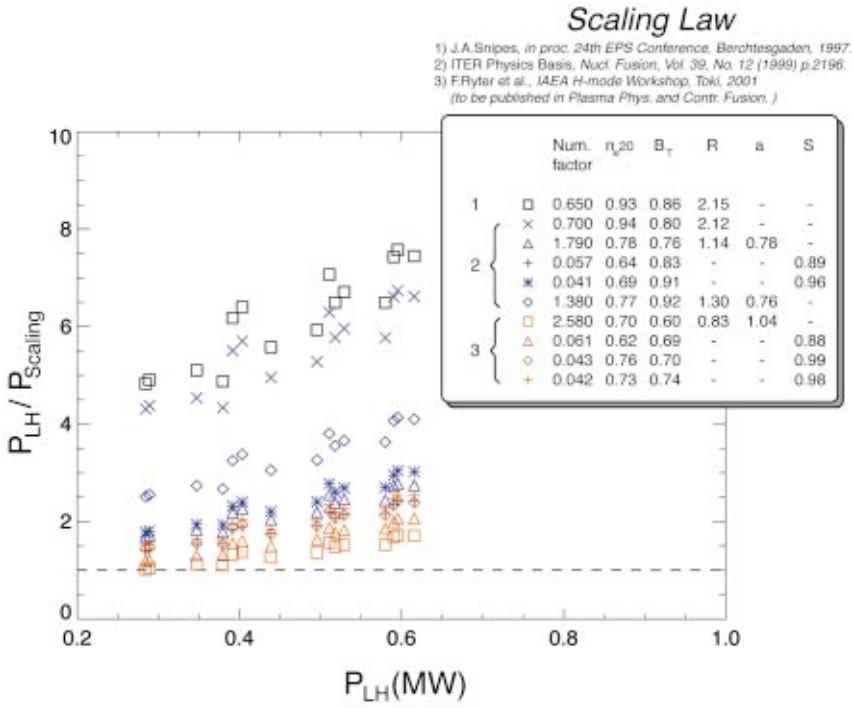

FIG. 6. (Color) Ratio of the L–H power threshold to scaling law prediction against P_{LH} for various scaling laws. The table contains the coefficients for the various scaling laws in the same form as expressed in Ref. 13, Table 2, p. 2196. Inboard gas-puffing and an adherence to the CDND plasma topology has resulted in good agreement with the latest scaling law predictions (shown in red) (Ref. 14).

for a subset of the Ohmic H-mode data and red points are for the NBI heated controlled density scan series (#4250–4265), showing a clear improvement in confinement as ELM frequency reduces, H_H exceeding 1.0 for low frequency ELMs. Black points are for a random selection (i.e., an uncontrolled set) of NBI heated H-mode plasmas; these also follow the trend. Data show a similar behavior to ELMy H-mode data in the presence of strong gas puffing in conventional tokamaks such as the Joint European Torus (JET) (Ref. 15). It appears then, that at densities approaching the Greenwald limit, the input power from a single, non-optimized beamline on MAST is not sufficiently above the threshold to produce Type I ELMs. Even so, it is interesting to note that $H_{\mathrm{IPB98(y,2)}}\sim 1$ is readily achievable for Type III ELMs; one can therefore anticipate significant improvements in the H_H factor when auxiliary heating powers of 3–4 MW become available in 2002 and Type I ELMs become accessible. As with the power-threshold data, MAST will provide a high leverage within the ITPA confinement and H-mode threshold database by providing an invaluable means of accurately extracting the aspect ratio regression coefficient (due to a doubling of inverse aspect ratio over the conventional machine database).

One particularly promising set of discharges (#4571–#4580) is highlighted in Fig. 7(a). These were generated in a series of experiments where the vertical field was ramped up in an attempt to maintain plasma position in the presence of strong NBI heating and rapidly rising β_p. This technique is being developed in order to sustain the plasma in the absence of an applied loop voltage from the solenoid. Figure 8 shows the time traces for discharge 4580. The L–H transition occurred at ~117 ms, after which point regular ELMs appeared and β_N started to rise at twice the rate usual for L-mode discharges. The ELMs had a frequency of ~0.55 kHz, had a very fast growth and decay, and do not appear to have generated the same degree of performance degradation as in other discharges at similar frequency [as evidenced in Fig. 7(a)]. Interestingly, the ELM frequency also decreases with an increasing line average density, in contrast to the majority of plasmas generated in 2001, perhaps indicative of Type I ELMs. H_H [w.r.t. IPB98(y,2)] for this discharge had an average value of around ~1.8, between discharge times 150 and 200 ms, with a maximum β_N of ~4.5. Also of note is that the bootstrap fraction for #4580 is estimated to be at the level $40\pm10\%$. Clearly though, these plasmas were inherently non-steady state. Indeed, the temporal derivatives of thermal and magnetic energies, the diamagnetic energy of the plasma, the fast ion stored energy and the plasma motion all had to be accounted for when determining the confinement time. At ~170 ms, a tearing mode appeared and the plasma performance started to degrade. Careful analysis, however, indicates that discharge 4571 did not contain such a prominent mode, but nevertheless underwent a similar beta collapse. The degradation in confinement (resulting at ~180 ms from changes to the Ohmic heating power, derivative terms in the Poynting flux calculation and later from a direct drop in β_N) appears instead to have been due to impurity influx (inferred from visible bremmstrahlung and impurity spectroscopy) and the fact that the vertical field ramp started to force the plasma against the center column. Experiments in 2002 will concentrate on utilizing upgrades to the feedback control system and increased auxiliary heating power to extend this high performance regime into a flat-top phase.

III. POWER HANDLING

Divertor power handling is a major challenge for the ST, due to the reduced major radius and consequently a smaller

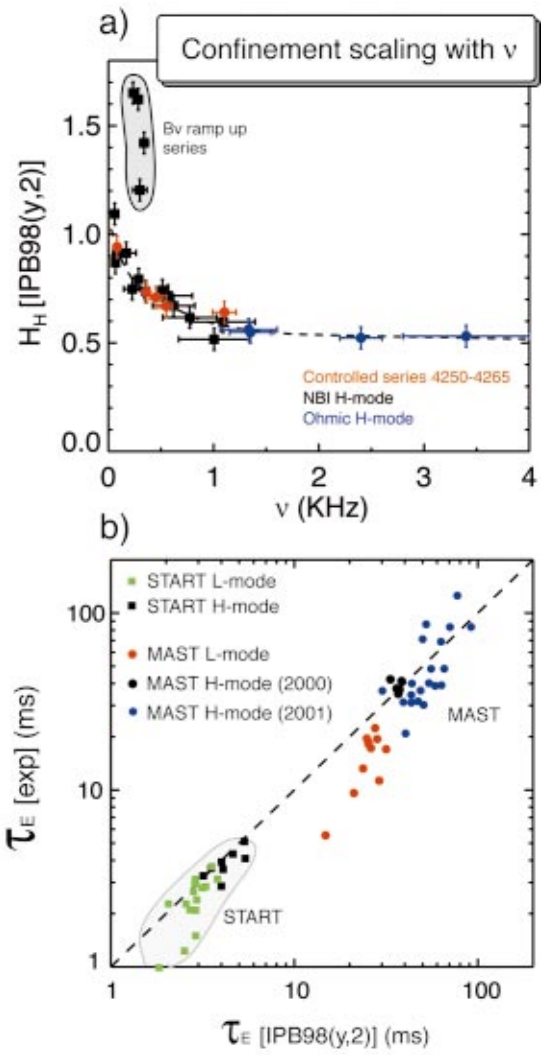

FIG. 7. (Color) (a) Confinement H_H factor [with respect to the international scaling IPB(*y*,2)] versus ELM frequency for various H-mode discharges. With the exception of the high performance vertical field ramp series, data show a similar trend to H-mode plasmas in the presence of strong gas puffing at a conventional aspect ratio. (b) shows the updated confinement scaling data for completeness.

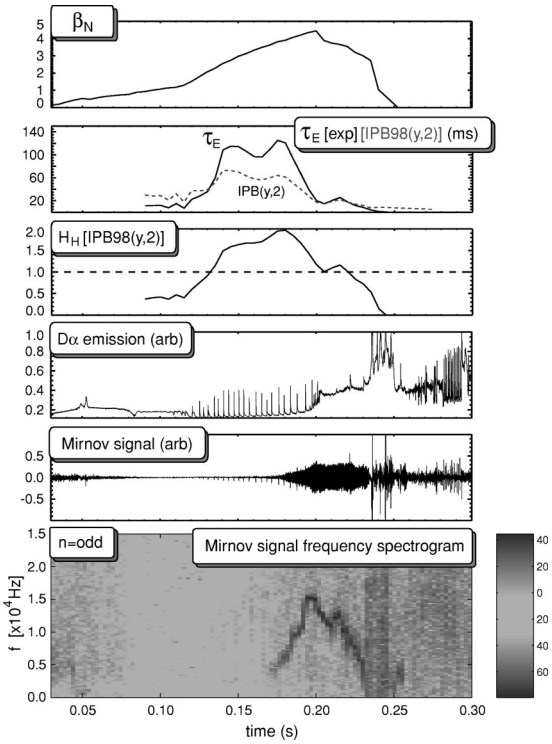

FIG. 8. Various time traces for discharge #4580, one of a series of high performance discharges whereby the plasma was sustained by ramping the vertical field without any applied voltage from the solenoid.

wetted area of the strike points. If the high performance plasmas described in the previous section are to be sustained in a next generation burning plasma device, or indeed in long pulse MAST scenarios, a sound understanding of the boundary and divertor plasma is paramount. Here, we briefly summarize some of the latest results concerning the potentially troublesome H-mode edge, in particular, addressing the issue of ELMs. A more detailed summary is given in Ref. 16.

MAST is well equipped with edge plasma diagnostics, including a high spatial resolution D_α array, a fast reciprocating probe at the outboard mid-plane, D_α views of all target structures and extensive arrays of high spatial and temporal resolution Langmuir probes. The probes have 3 mm inboard spacing, 10 mm spacing outboard and are multiplexed at a 65 μs sweep (much less than the ELM period), once per millisecond. To obtain target profiles both at the ELM peaks and inter-ELM during regularly ELMing H-mode, box-car techniques are utilized.

The power arriving at each of the target probes, P^t, is evaluated from the saturation current, j_s, and electron temperature, T_e, using $P^t = \gamma k T_e j_s / e$. Here we take the sheath transmission coefficient $\gamma = 7$ (the sum of the electron and ion sheath transmission coefficients, estimated for deuterium ions and a graphite target, assuming $T_i \sim T_e \sim 20$ eV and accounting for secondary electron emission, electron–ion recombination and ion particle and energy reflection coefficients). Molecular recombination has a negligible impact and has been ignored. Exponential fits to P^t in both the SOL and private flux regions at each of the four strike points are applied in order to derive the target heat flux scale lengths, $\lambda_P^{t,\mathrm{SOL}}$ and $\lambda_P^{t,\mathrm{PFR}}$. The total power flowing to each target is then evaluated by integrating over the strike point regions using $P^t_{\mathrm{tot}} = 2\pi R_s P^t_{\mathrm{peak}} (\lambda_P^{t,\mathrm{SOL}} + \lambda_P^{t,\mathrm{PFR}})$, where R_s is the strike point radius and P^t_{peak} is the value of P^t at the intersection of the two exponential fits. For comparison, P^t_{tot} has also been evaluated directly from P^t at each probe using a Simpson's rule integration approach. Typically, the exponential fitting and Simpson's rule values agree to within 10% and the total power to all four targets routinely matches the power crossing the separatrix (calculated using EFIT) with an accuracy of ~20%.

Figure 9(a) shows target peak electron densities for the inner and outer divertor legs, averaged between the upper and lower targets as a function of the line averaged core electron density for a set of L-mode plasmas. Closed points are for $P_{\mathrm{sep}} < 1$ MW and open points for $P_{\mathrm{sep}} > 1$ MW. Here,

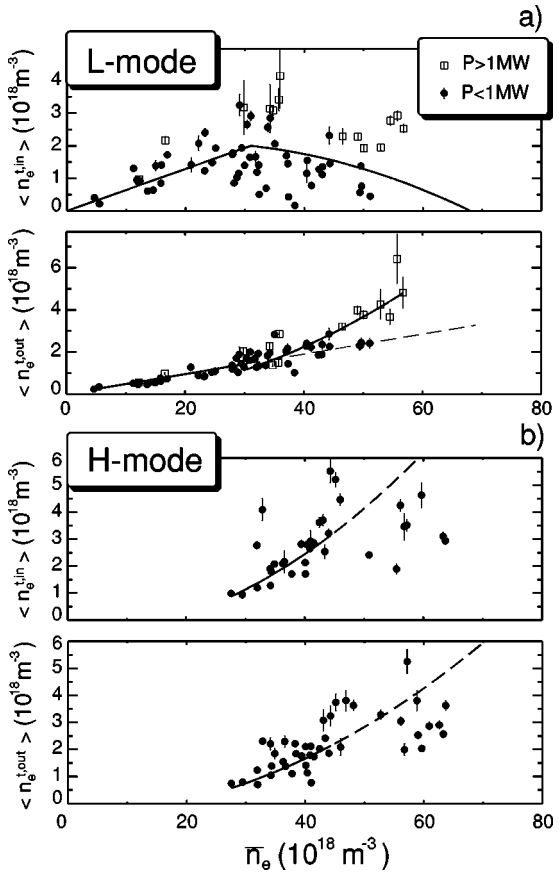

FIG. 9. Target peak electron densities as a function of line average electron density for L- (a) and H-mode (b) plasmas. For the H-mode discharges, data were taken at the ELM peak.

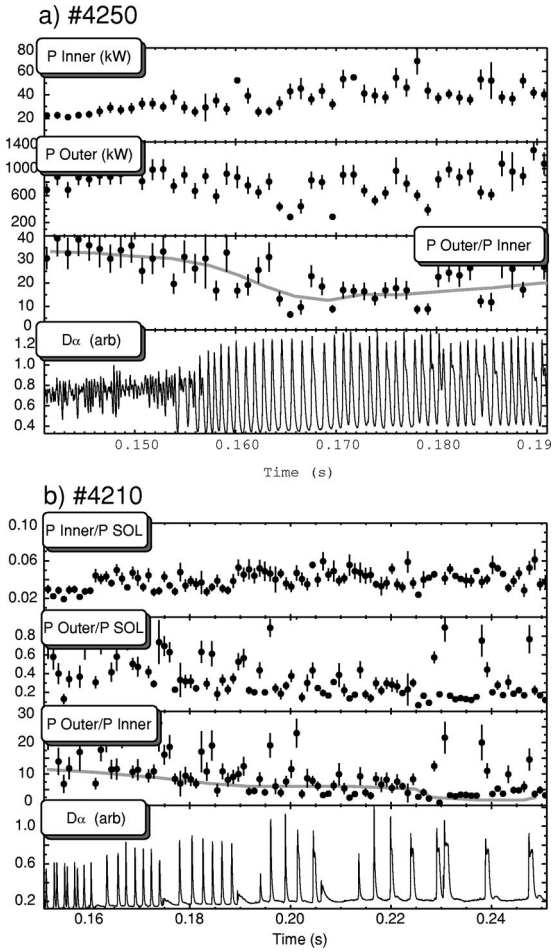

FIG. 10. Power loading asymmetry and D_α in discharges #4250 (a) and #4510 (b).

P_{sep} is defined as the total power crossing the separatrix assuming electron–ion equipartition. Considering first the outer targets, a clear linear rise with n_e^{out} from $2\times10^{17}/m^3$ to around $10^{18}/m^3$ takes place over the range $5\times10^{18}<\bar{n}_e<3\times10^{19}/m^3$, indicative of "low recycling" (for a description see Ref. 17). For higher densities, n_e^{out} and n_e^{in} deviate from the linear fit and are instead best parametrized by a quadratic relationship $n_e^{out}\propto n_e^2$, indicating the onset of "high recycling" above $3\times10^{19}/m^3$. The inner targets show similar behavior up to $n_e\sim3-4\times10^{19}/m^3$ but in contrast, for $\bar{n}_e>4\times10^{19}/m^3$, n_e^{in} begins to fall with increasing $\bar{n}_e$, more markedly for the lower power cases where n_e^{in} drops to around $5\times10^{17}/m^3$ at $\bar{n}_e\sim5\times10^{19}/m^3$. Inboard data for L-mode plasmas are thus consistent with the onset of detachment for $\bar{n}_e>3.5\times10^{19}/m^3$, becoming fully detached for cases with $P_{sep}<1$ MW at $\bar{n}_e\geqslant5\times10^{19}/m^3$.

Figure 9(b) shows the equivalent plots for H-mode plasmas (data taken at the ELM peak, although broadly similar results are obtained in between ELMs). Perhaps not surprisingly, data are more scattered in the H-mode due to box-car averaging over the ELMs, thus preventing a clear determination of the relationship between the target densities and $\bar{n}_e$. However, a comparison of n_e^{out} in the H-mode and the L-mode suggests that the outboard SOL in the ELMy H-mode is in an attached, low recycling regime up to the highest $\bar{n}_e$ so far explored. For the inboard targets, the lack of a rollover in n_e^{in} (supported by electron temperature data showing $T_e^{in}>10$ eV) indicates that they remain in an attached regime up to the highest densities so far explored. Characterization of the MAST SOL in high power ELMy H-mode is continuing, in particular, upstream data from a reciprocating probe and onion-skin modeling of the SOL are being used to develop parameter scalings for the heat flux SOL width in MAST.

In Ref. 5 we reported that in the ELM free H-mode, the outer–inner separatrix power flux asymmetry drops from an L-mode value of ~20 to a level close to the ratio of outer to inner separatrix areas (~4), indicative of the suppression of ballooning-like turbulence. Routine access to ELMing H-mode is now facilitating such studies in regimes closer to steady state. Figure 10(a) shows time traces of the power crossing the outer and inner separatrices, the outer–inner power asymmetry and a D_α trace for H-mode discharge #4250, the L–H transition occurring at ~154 ms.

On transition to Type III regularly ELMing H-mode ($f_{ELM}\sim1$ kHz), the power asymmetry fell from ~35 to an average level of around 15–20, mostly as a result of a rise in P_{in} during the ELMing phase. Broadly speaking, as f_{ELM} decreases [with increasing power for instance as mentioned in Sec. II), the power asymmetry is seen to fall, approaching

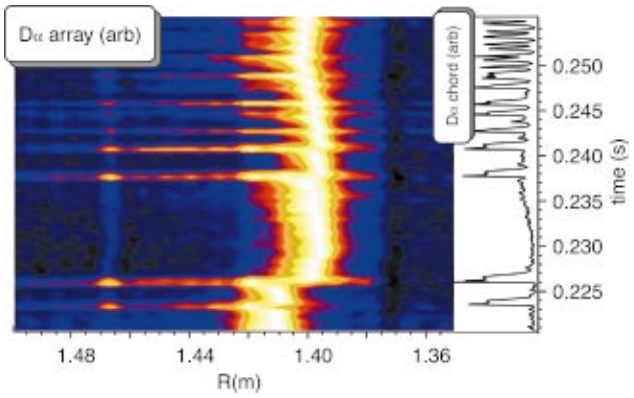

FIG. 11. (Color) Mid-plane radial D_α emission and D_α emission in the divertor as a function of time in ELMing H-mode. The ELM structure is seen to extend ~8–10 cm outside the separatrix.

the ELM free H-mode value of ~4 during inter-ELM periods, as seen for discharge #4510 in Fig. 10(b)]. At the ELM peaks, the power asymmetry transiently returns to around 20, although some are missed due to probe multiplexing. More detailed experiments are described in Ref. 16. In MAST, the peak heat flux during ELMs has not exceeded 8 $MW\,m^{-2}$, even at the lowest observed ELM frequencies (which may exhibit Type I characteristics). The outboard asymmetry in the deposition of Type III ELM energy observed in MAST DND plasmas, is potentially very favorable for the spherical tokamak concept. Under these conditions, the bulk of ELM energy is delivered to the outer divertor (where wetted areas in a burning ST device could be up to two orders of magnitude larger than at the inboard targets). Of course, it remains to be seen whether this power asymmetry remains after a transition to a clearly defined Type I ELMy H-mode.

The future success of the tokamak will clearly benefit from a greater understanding of the ELM instability itself. To this end, a newly commissioned mid-plane mounted fast reciprocating probe is being combined with linear D_α array data, passive spectroscopy, turbulence reflectometry and target probe arrays in order to study directly the detailed dynamics of the ST ELM. Figure 11 shows a tomographically inverted, false color image of the D_α emission from an ELMy H-mode plasma #4548, together with a divertor D_α trace. The intensity has been normalized to the peak value at each time slice to aid the eye. Inter-ELM, the profile is Gaussian with a typical half-width of 2–3 cm. During the ELMs themselves, however, the emission becomes strongly skewed towards the outboard side (to the left), the emission profile remaining more or less the same inside the separatrix but displaying a long tail which extends some ~10–20 cm outside the plasma. Indeed, if the reciprocating probe is placed too close to the plasma, ELMs can interact strongly with the probe and trigger H–L transitions or in the worst cases, plasma disruption. Data from the reciprocating probe at ~17 cm from the plasma edge, indicate that the saturation current J_s reaches up to 50 kA/m^2, similar to levels at the target probes during ELMs. In addition, timing information indicates that the saturation current J_s at the reciprocating probe rises much more rapidly than the divertor D_α spike but lags behind it by around 350 μs. Combined, data suggest that the ELMs are associated with a rapid, radially outwards motion ($V \sim 300-500$ m/s) of a poloidally and/or toroidally localized structure. Data are clearly of rather a preliminary nature, and it is hard to draw firm conclusions at this stage. Nevertheless it is of note that the existence of ''blobs'' or ''filaments'' has been used to explain observations of small scale turbulent losses in a range of tokamaks (see, for example, Refs. 18 and 19) and an extension to ELM transients may be in order.

IV. OPERATIONAL LIMITS

Thus far, the emphasis on MAST has been to develop mainstream operating regimes for L and H-mode plasmas, rather than to explore density, beta or q-limits. Even so, an increase in 2001 of the available NBI power (up to 1.7 MW, 34% of the design goal) has enabled significant progress to be made in generating plasmas with high beta and high density. Figure 12(a) shows the Troyon beta space diagram for year 2001 discharges. Here, discharge trajectories have been binned and a contour algorithm applied, the color thus representing the amount of time discharges spend in a given part of parameter space. The highest β_N parameters were achieved for series #4580, described in Sec. II (non-solenoid

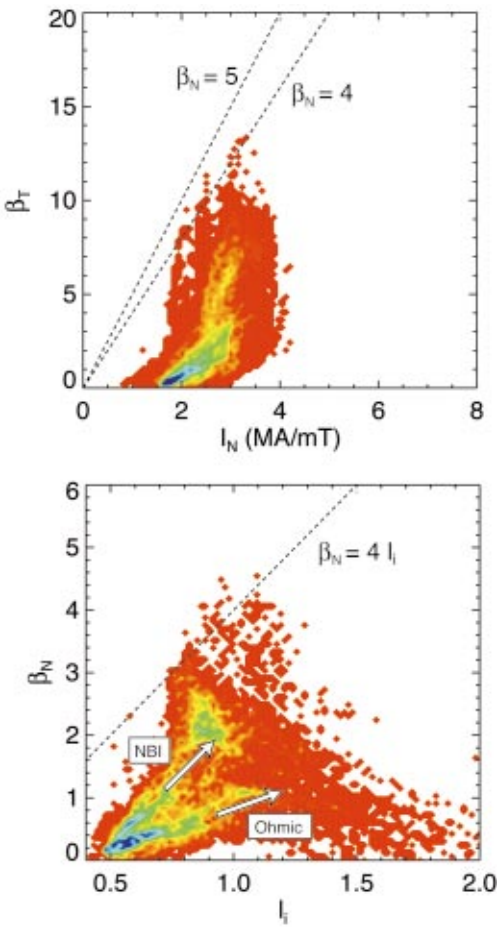

FIG. 12. (Color) Beta operating space (binned discharge trajectory contour plots) for year 2001 MAST discharges. The color represents the amount of time MAST plamsas spend in a given part of parameter space.

current drive experiments requiring high values of βp). Values of β_N up to 4.5 and β_T up to ~13% have been achieved, exceeding the empirical DIII-D no-wall limit $\beta_N = 4l_i$ [Fig. 12(b)] and showing a similar trend to results from the U.S., National Spherical Torus Experiment NSTX (see, for example, Ref. 20). To date, there has been no evidence of pressure driven disruption; prospects remain high then that β_T can be raised further with planned increases in the available auxiliary heating power, thus probing the high values theoretically achievable in the ST.

We have already discussed a number of issues associated with operational limits in the H-mode, in particular power thresholds, increased accessibility due to inboard gas fueling and the performance limits imposed by ELMs. We now turn to a discussion of the density operating space spanned by MAST plasmas and describe the latest attempts at increasing the H-mode density using low field side (LFS) pellet injection. In the first operational campaign, MAST plasmas with Greenwald numbers in excess of 1.0 were obtained for plasma currents up to 0.55 MA (data being reported in Sec. 6 of Ref. 21). More recently, extended discharge duration and increases in the available beam power have extended the operating space for gas puff fueled discharges to $G>1$ for I_p up to ~0.8 MA (Fig. 13). Greenwald numbers as high as 1.8 have been achieved and there is as yet no evidence of a clearly defined density limit, the ST plasma appearing resilient to density limit disruptions. Indeed, poloidally localized MARFEs (Multi Faceted Radiation from the Edge) occasionally appearing at $G>0.95$ do not seem to cause radiative collapse of the plasma column or limit the achievable density.

A multi-pellet injection system has recently been installed, preliminary results having been obtained using low field side mid-plane launch and D_2 fuel pellets with a deuterium drive gas. Up to 8 pellets per discharge are available, with particle inventories per pellet of typically between 0.5×10^{20} and 2×10^{20} and vessel entry velocities in the range 400–600 m/s.

Figure 14 shows time traces for a typical 1.0 MA NBI heated H-mode discharge (#4487). Beam heating began at 30 ms and terminated at 280 ms. The L–H transition took place

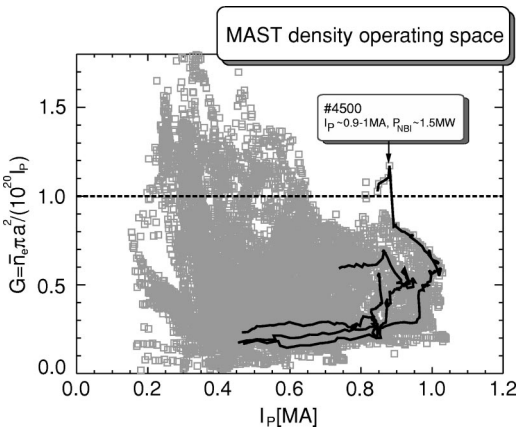

FIG. 13. MAST density operating space with three pellet fueled trajectories overlaid.

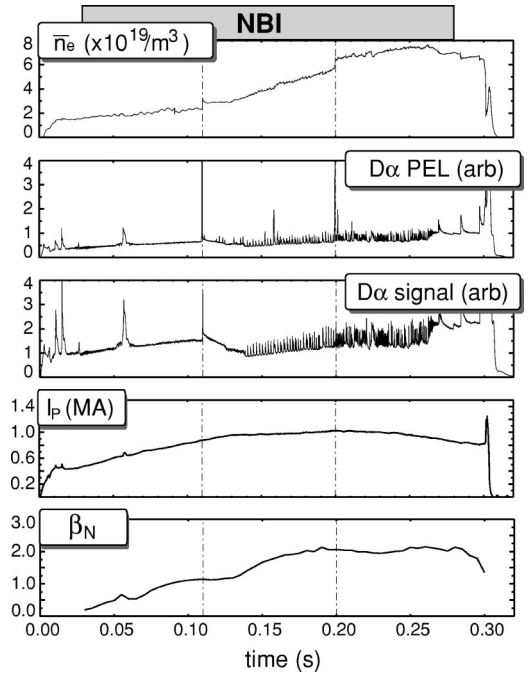

FIG. 14. Time traces for pellet fueled H-mode discharge #4487. A clear increase in line average density is evident at each pellet injection (marked by the vertical dotted lines).

at around 135 ms with the onset of ELMs (evident from the divertor and pellet line of sight D_α traces). The first pellet to be injected was a medium sized pellet (1.7×10^{20} atoms) with velocity 641 m/s (both measured at the injector), incident during the L-mode phase of the discharge at 110 ms, the beta trace indicating that the absorption was close to adiabatic. The estimated fueling efficiency for this pellet is 25%, significantly lower than for Ohmic L-mode plasmas where the fueling efficiency is high at over 75%. This low efficiency may be associated with the higher plasma temperature, the presence of a significant fast ion population (the consequence of which has yet to be quantified) and the absence of a high beta magnetic valley (see Ref. 22) (which in theory can enhance the inwards E×B drift of the pellet cloud). The second pellet entered during the H-mode at 200 ms. At the injector, the pellet was large (3.7×10^{20} atoms), with a velocity 535 m/s, but split into two during flight. Even so, the resulting pellet ablation time of 0.75 ms was similar to that for the first pellet, and particle retention was more favorable (inferred from the interferometer signal), an expected result due to the higher particle confinement associated with the H-mode. Three pellet shots are included as discharge trajectories in Fig. 13, 1 MA H-mode discharge 4500 ($P_{\mathrm{NBI}}=1.7$ MW) so far having shown the highest performance. The density of this plasma was ratcheted up using 4 pellets, exceeding $G>1$ for 20 ms.

V. H-MODE STABILITY AND THE NEOCLASSICAL TEARING MODE

A key benefit of the ST is its access to high beta, based upon arguments of ideal MHD stability (for a discussion see Ref. 23 or 24), and demonstrated experimentally on the

START device (which transiently reached $\beta_T \sim 40\%$, Ref. 8). Two categories of MHD may potentially stymie the access to power-plant level betas (for a typical ST power-plant design see Ref. 25). Fast particle driven instabilities such as Toroidal Alfvén Eigenmodes (TAEs) are a concern, due to the high densities and low fields characteristic of the ST plasma, and have indeed been observed on MAST; they are, however, rare, and as yet do not seem to be accompanied by any performance degradation. Conventional tokamaks are often limited by another MHD instability, the Neoclassical Tearing Mode (NTM) (discussed in Refs. 3, 4, and 26) which occurs below the ideal MHD beta limit in hot, low collisionality plasmas. The new generation of STs access this low collisionality regime for the first time in a low aspect ratio plasma, and hence, by operating MAST in regimes with large sawteeth, low collisionality ($\nu = \nu_i / \varepsilon \omega_{e*} \sim 0.05$ where ν_i is the ion collisionality, ε is the inverse aspect ratio and ω_{e*} is the electron diamagnetic frequency, all calculated locally at the $q = 3/2$ surface) and high poloidal beta, it is possible to trigger NTMs, providing the first studies of their behavior at low aspect ratio.

In these scenarios, sawtooth triggered 3/2 and 2/1 NTMs are frequently observed (m/n denoting the poloidal/toroidal mode numbers). Mode numbers are clearly identified by poloidal and toroidal magnetic arrays, with observed poloidal structure confirmed by modeling. The 3/2 NTM has a modest impact upon performance, whilst large 2/1 NTMs are often associated with a transition from H- to L-mode and, subsequently, disruption. Mode activity usually appears in H-mode, the 2/1 NTM tending to lock periodically if present in L-mode plasmas. Typical island sizes are ~4 cm for the 3/2 NTM and 10 cm for the 2/1, deduced from estimates using a cylindrical model and in good agreement with both detailed field line tracing calculations and (for the 2/1) local flattening observed in Thomson scattering profile measurements.

An example is shown in Fig 15. Here, each sawtooth acted as a seed, exciting $n=2$ islands (which then decayed), but once high enough β_p was reached, a rapid growth of a 3/2 NTM took place, resulting in a fall of 3 kJ in thermal energy compared to pre-NTM trend values. This compares with a 2.4 kJ loss predicted by the Chang and Callen belt model (described in Ref. 27) (based upon pressure flattening across the island width). As β_p fell, the mode decayed, but on entry into H-mode, a 2/1 NTM was excited, ultimately locking and disrupting the plasma. Generally modes are excited close to their "critical β_p" (below which NTMs are unconditionally stable), indicating a strong seeding process. This is likely to be associated with the large inversion radius of the sawteeth and tight aspect ratio of the ST.

To explore the underlying physics in more detail, experiments with a controlled termination of the NBI power have been carried out in order to study the decay of the mode following the resulting fall in β_p. A typical island evolution is shown in Fig. 16. The steady amplitude early on (in the presence of bootstrap currents due to high β_p) indicates a negative Δ' (the classical tearing stability index). Modeling (smooth curves) with the usual form of the modified Rutherford equation (as given in Ref. 28) shows a remarkable match to the theoretically expected behavior. The inclusion of small island size stabilization terms, from ion polarization currents (Ref. 29) and/or finite island transport (Ref. 30), is required to explain the strong decay in amplitude as β_p falls, leading to the curves labeled "w_{pol}" and "w_d." In both cases the bootstrap coefficient requires only modest (+8%) adjustment from the theoretically calculated value (using parametric fits from Ref. 31). It is, however, necessary to include stabilizing field curvature effects, calculated (from theory outlined in Ref. 32) to cancel out ~60% of the bootstrap drive in these discharges, providing a first validation of the effects of field curvature physics. Further details can be found in Ref. 33.

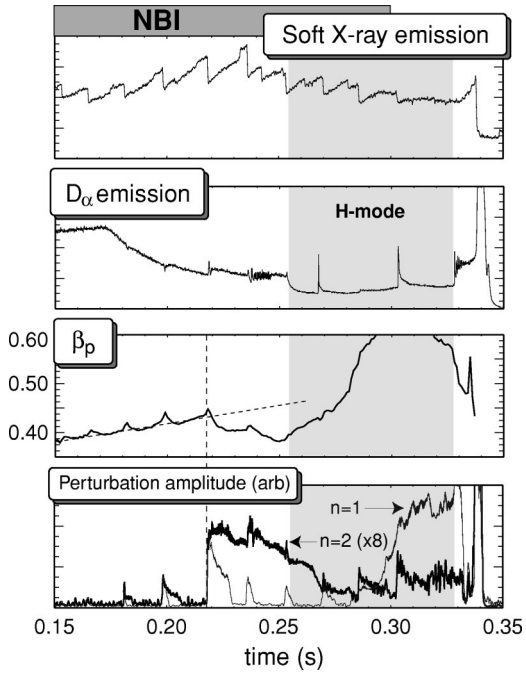

FIG. 15. Time traces for discharge 2941, highlighting 2/1 and 3/2 NTM behavior and the resulting effect upon confinement (from β_P).

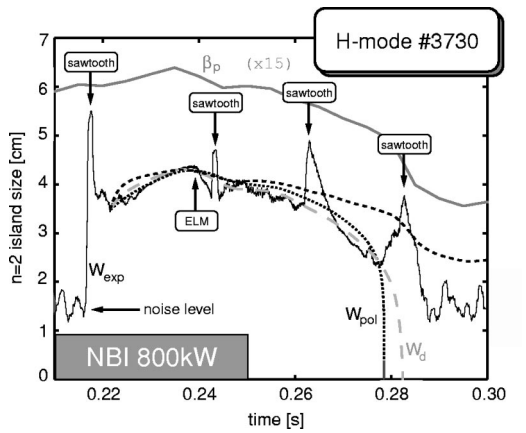

FIG. 16. Evolution of an $n=2$ island in the presence of decaying β_P. Model predictions labeled W_{pol} (for the polarization current model) and W_d (for the finite island transport model) are seen to agree well with the experimental data provided finite island size stabilization and field curvature effects are included.

VI. SUMMARY

In summary, H-mode access in Ohmic and NBI heated discharges (both limiter and X-point diverted) is now routine on MAST. Approximately 35% of all discharges in the 2001 campaign of operation contained an H-mode phase with regular ELMs. Careful studies, whereby subtle changes to the plasma topology have been effected, indicate that the power threshold in Connected Double Null plasmas with inboard gas fueling is the lowest ($\delta \sim 0.4$), enabling Ohmic H-mode plasmas to be generated for the first time in a ST. The resulting power threshold, although for double null plasmas with an open divertor structure, is now broadly consistent with the latest international power law scalings. The ELMs themselves appear to be predominantly Type III, demonstrating the expected scalings with line average density and power crossing the separatrix. Confinement for low frequency Type III ELMs is in agreement with the international scaling law IPB(y,2) and degrades with increasing ELM frequency, in line with data from conventional tokamaks. A handful of high performance but nonsteady state Neutral Beam Heated discharges fall outside the usual trend, demonstrating H_H factors [w.r.t. IPB(y,2)] of up to ~ 2, the high confinement leading to $\beta_N \sim 4.5$ with a bootstrap fraction of around 40%. Attempts will be made in 2002 to extend these plasmas into the flat-top regime. The large complement of edge diagnostics on MAST is allowing detailed studies of the H-mode pedestal. In particular, the outboard asymmetry in the deposition of Type III ELM energy in MAST DND plasmas is potentially very favorable for the ST concept, as the bulk of the power in a burning plasma should be incident upon the much larger outboard wetted areas. Even at the lowest ELM frequencies the inboard targets on MAST have not received more than 8 MW/m^2 (ELM peak) of power flux. We have reported the first results from a newly installed low field side mid-plane launch pellet injector. Data from the limited number of pellet enhanced discharges so far recorded are very promising. The ablation process appears to be adiabatic and the Greenwald limit has now been exceeded for plasma currents up to 0.9 MA. Due to the available beam power having so far been limited to <1.7 MW, beta limit studies have not yet been attempted. High performance H-mode discharges are at sufficient beta, however, to provide the first glimpse of the Neoclassical Tearing Mode in ST geometry. The physics of the NTM in the ST appears to be similar to that seen at conventional aspect ratio, modeling highlighting the role of stabilizing field curvature terms, which are much stronger in the ST than in conventional tokamaks. Results from MAST continue to support and extend the understanding of basic tokamak behavior relevant to the ITER program and, in addition, show promise for the future application of the ST as a potential fusion device.

ACKNOWLEDGMENTS

This work was funded by the UK Department of Trade and Industry and by EURATOM. The NBI equipment is on loan from ORNL and the pellet injector was provided by FOM.

[1] A. C. Darke, J. R. Harbar, J. H. Hay *et al.*, *Fusion Technology 1994, Proceedings of the 18th Symposium on Fusion Technology*, Karlsruhe, Germany, 22–26 August 1994 (Elsevier, Amsterdam, 1995), Vol. 1, p. 799.
[2] Y. K. M. Peng and D. J. Strickler, Nucl. Fusion **26**, 769 (1986).
[3] Z. Chang, J. D. Callen, E. D. Fredrickson *et al.*, Phys. Rev. Lett. **74**, 4663 (1995).
[4] R. Carrera, R. D. Hazeltine, and M. Kitschenreuther, Phys. Fluids **29**, 899 (1986).
[5] R. Akers, G. F. Counsell, A. Sykes *et al.*, Phys. Rev. Lett. **88**, 035002 (2002).
[6] M. Valovic, S. J. Fielding, P. G. Carolan, B. Lloyd, M. Price, V. Shevchenko, S. You, and M. J. Walsh, *Proceedings of the 28th EPS Conference*, Madeira, 2001 (European Physical Society, Geneva, 2001), Vol. 25A, p. 1829.
[7] A. Field *et al.*, "H-mode plasmas in the MAST spherical tokamak," *Proceedings of the IAEA H-mode Workshop*, Toki, September 2001, to appear in Plasma Phys. Controlled Fusion.
[8] A. Sykes, R. J. Akers, L. C. Appel *et al.*, Phys. Rev. Lett. **84**, 495 (2000).
[9] J. W. Connor, Plasma Phys. Controlled Fusion **40**, 531 (1998).
[10] H. Meyer *et al.*, "The effect of magnetic configurations on H-mode in MAST," Phys. Rev. Lett. (submitted).
[11] T. N. Carlstrom, R. J. Groebner, and T. L. Rhodes, Bull. Am. Phys. Soc. **46**, 220 (2001).
[12] *Proceedings of the 24th EPS Conference, Berchtesgaden 1997* (European Physical Society, Geneva, 1997), Vol. 3, p. 961.
[13] ITER Physics Basis, Nucl. Fusion **39**, 2137 (1999).
[14] F. Ryter *et al.*, "Progress of the International H-Mode Power Threshold Database Activity," in Ref. 7.
[15] G. M. Fishpool, Nucl. Fusion **38**, 1373 (1998).
[16] G. F. Counsell, A. Kirk, J.-W. Ahn, A. Tabasso, and Y. Yang, Plasma Phys. Controlled Fusion **44**, 1 (2002).
[17] P. C. Stangeby, *The Plasma Boundary of Magnetic Fusion Devices* (Institute of Physics, Bristol, UK, 2000).
[18] S. Krasheninnikov, Phys. Lett. A **283**, 368 (2001).
[19] S. J. Zweben, D. P. Stotler, J. L. Terry *et al.*, Phys. Plasmas **9**, 1981 (2002).
[20] S. Sabbagh, R. E. Bell, M. G. Bell *et al.*, Phys. Plasmas **9**, 2085 (2002).
[21] A. Sykes, J.-W. Ahn, R. Akers *et al.*, Phys. Plasmas **8**, 2101 (2001).
[22] D. R. Mikkelsen, R. B. White, R. J. Akers, S. M. Kaye, D. C. McCune, and J. E. Menard, Phys. Plasmas **4**, 3667 (1997).
[23] J. A. Wesson and A. Sykes, Nucl. Fusion **25**, 85 (1985).
[24] F. Troyon *et al.*, Phys. Lett. A **110**, 29 (1985).
[25] R. Akers *et al.*, Nucl. Fusion **40**, 1223 (2000).
[26] R. J. Buttery *et al.*, Plasma Phys. Controlled Fusion **42**, B61 (2000).
[27] Z. Chang *et al.*, Nucl. Fusion **34**, 1309 (1994).
[28] O. Sauter, R. J. La Haye, Z. Chang *et al.*, Phys. Plasmas **4**, 1654 (1997).
[29] H. R. Wilson, J. W. Connor, R. J. Hastie, and C. C. Hegna, Phys. Plasmas **3**, 248 (1996).
[30] R. Fitzpatrick, Phys. Plasmas **2**, 825 (1995).
[31] O. Sauter, C. Angioni, and Y. R. Lin-Liu, Phys. Plasmas **6**, 2834 (1999).
[32] H. Lutjens, J.-F. Luciani, and X. Garbet, Phys. Plasmas **8**, 4267 (2001).
[33] R. Buttery, O. Sauter, R. Akers, M. Gryaznevich, R. Martin, C. D. Warrick, and H. R. Wilson, Phys. Rev. Lett. **88**, 125005 (2002).